Modeling the complexity of acoustic emission spectra during intermittent plastic deformation: Power laws and multifractal spectra

2 authors:

Jagadish Kumar
...
28 PUBLICATIONS   179 CITATIONS

SEE PROFILE

G. Ananthakrishna
Indian Institute of Science
175 PUBLICATIONS   2,757 CITATIONS

SEE PROFILE

Some of the authors of this publication are also working on these related projects:

Carbon stock assessment in Similipal Biosphere Reserve View project

Dislocation dynamical approach to nano-indentation instabilities. View project

Modeling the complexity of acoustic emission during intermittent plastic deformation: Power laws and multifractal spectra

Jagadish Kumar[1] and G. Ananthakrishna[2]

[1]*Department of Physics, Utkal University, Bhubaneswar 751004, India*
[2]*Materials Research Centre, Indian Institute of Science, Bangalore 560012, India*

Scale-invariant power-law distributions for acoustic emission signals are ubiquitous in several plastically deforming materials. However, power-law distributions for acoustic emission energies are reported in distinctly different plastically deforming situations such as hcp and fcc single and polycrystalline samples exhibiting smooth stress-strain curves and in dilute metallic alloys exhibiting discontinuous flow. This is surprising since the underlying dislocation mechanisms in these two types of deformations are very different. So far, there have been no models that predict the power-law statistics for discontinuous flow. Furthermore, the statistics of the acoustic emission signals in jerky flow is even more complex, requiring multifractal measures for a proper characterization. There has been no model that explains the complex statistics either. Here we address the problem of statistical characterization of the acoustic emission signals associated with the three types of the Portevin–Le Chatelier bands. Following our recently proposed general framework for calculating acoustic emission, we set up a wave equation for the elastic degrees of freedom with a plastic strain rate as a source term. The energy dissipated during acoustic emission is represented by the Rayleigh-dissipation function. Using the plastic strain rate obtained from the Ananthakrishna model for the Portevin–Le Chatelier effect, we compute the acoustic emission signals associated with the three Portevin–Le Chatelier bands and the Lüders-like band. The so-calculated acoustic emission signals are used for further statistical characterization. Our results show that the model predicts power-law statistics for all the acoustic emission signals associated with the three types of Portevin–Le Chatelier bands with the exponent values increasing with increasing strain rate. The calculated multifractal spectra corresponding to the acoustic emission signals associated with the three band types have a maximum spread for the type C bands and decreasing with types B and A. We further show that the acoustic emission signals associated with Lüders-like band also exhibit a power-law distribution and multifractality.

I. INTRODUCTION

It is well known that the motion of dislocations is inherently intermittent with waiting periods at junctions where they are arrested followed by nearly free flights between them. This feature is not reflected during the homogeneous yield phenomenon where the stress-strain (σ-ϵ) curves are smooth. However, the intermittent behavior reappears as serrations on the stress-strain curves when the diameter of the rod is decreased below a fraction of a micron, confirming the inherently intermittent character of dislocation motion [1,2]. On the other hand, jerky flow or the Portevin–Le Chatelier (PLC) effect is observed at macroscopic scales when specimens of dilute alloys are subjected to constant strain rate deformation [3,4]. The intermittent deformation manifests itself as a series of serrations on the stress-strain curves in a range of temperatures and strain rates. A standard explanation is that the discontinuous flow is due to collective pinning and unpinning of dislocations from the solute cloud. Clearly, the underlying dislocation mechanisms must necessarily be different in these two cases.

The acoustic emission (AE) technique has long been used as a tool to probe the dynamics of dislocations on finer scales in several kinds of deformation studies, in particular, in the two cases mentioned above. For instance, AE studies on the smooth homogeneous yield phenomenon exhibit intermittent AE signals with its overall envelope exhibiting a peak just beyond the elastic regime decaying for larger strains [5,6]. Recent AE studies for this case throw light on the origin of the pulselike character of AE signals [7–10]. The smooth σ-ϵ curves are then interpreted as resulting from the averaging process of the dislocation activity in the sample.

Acoustic emission studies carried out for over five decades have established specific correlations between the nature of the AE signals and the nature of stress-strain curves for different situations [5,6,11–17]. The nature of the AE signals in the case of discontinuous flow where the stress-strain curves display stress serrations is qualitatively different from that for the continuous homogeneous yield. For example, studies on the PLC effect have established specific types of correlations between the nature of the AE signals and the three different types of bands and the associated serrations [10,11,13–15,18,19]. For the uncorrelated static type C bands that displays large-amplitude serrations, the AE signals consist of well separated AE bursts with a low-level AE background, while for the partially propagating type B bands exhibiting relatively small-amplitude serrations, the AE bursts begin to overlap. The AE signals corresponding to the fully propagating type A bands (with very-small-amplitude serrations) are continuous with bursts of AE appearing only occasionally [13–15,19]. These

characteristic features have been captured in our recent work [20,21]. Similar correlations exist for the Lüders band [14–17], another type of propagative instability [22]. Furthermore, the AE signals for the Lüders band are different from that for the three PLC bands [3,4], a feature that is also captured by our model [21].

In the case of propagative instabilities, collective dislocation processes govern the nature of the bands and the associated stress-strain curves. While the AE associated with both the continuous yield and the discontinuous yield consists of a sequence of intermittent bursts of acoustic energy, the AE technique is able not only to distinguish these two types of AE patterns, but also to quantify them. Indeed, the recent progress in experimental techniques with a high degree of resolution and accuracy has helped to establish quantitative characterization of the AE signals corresponding to the different types of stress-strain curves [7,9,10,14,15,23,24].

One characteristic feature of AE signals is the scale-free statistics of the amplitude (or energy) in widely different physical systems such as volcanic activity [25], microfracturing processes [26], thermal cycling of martensites [27–29], peeling of an adhesive tape [30–32], and plastic deformation of materials exhibiting homogeneous yield [7,9,10] as well as discontinuous flows [10,23,24]. In the context of plastic deformation, the statistics of the recorded intermittent AE signals obtained from a uniaxial compressive creep of ice crystals, e.g., single and polycrystalline samples of hcp and fcc structures [10], follow power-law distributions. Surprisingly, even in the case of the PLC effect, power-law distributions for the AE energies are reported for all the PLC bands [10,19,24]. Interestingly, while the scaling region for the AE energies corresponding to the type A bands is the lowest scaling regime, it is only for the type A band that power-law distributions for the magnitudes and durations of stress drops have been reported [23,33–35].

The fact that power-law distributions of the AE signals are seen in these two cases (of homogeneous and discontinuous flows) with distinctly different dislocation dynamics is surprising. The power-law statistics for the homogeneous yield has been predicted in two- and three-dimensional simulations [9,36]. The underlying physical mechanism is the formation of dislocation network that is driven to the edge of criticality. In this state, some proportion of the network is poised at and just below the criticality. Then bursts of AE are attributed to the coherent unpinning of those dislocation segments at criticality. Once unpinned, these segments are arrested falling below the critical state with segments below the criticality pushed to the threshold, much like the sandpile model scenario [37]. Clearly, this kind of explanation cannot hold for the power-law statistics of the AE signals associated with the PLC bands since these band types are attributed to collective unpinning of dislocations. We are unaware of models or simulations that predict the power-law statistics of the AE signals in the case of the PLC effect. Thus, our primary objective is to examine if the calculated model AE signals associated with the three PLC bands [21] exhibit power-law statistics.

Even more interesting is the fact that the statistical properties of the AE signals from the PLC bands are even more complex, requiring a distribution of scaling exponents for a proper characterization, unlike the single exponent required for

characterizing a power-law distribution [10,19,24]. Indeed, the statistical properties of such complex sets are mathematically characterized by a continuum of generalized Rényi dimensions D_q parametrized by a parameter q [38–40]. Alternately, they can be described as an interwoven sets of Hausdorff (fractal) dimensions $f(\alpha)$ having a singularity strength α [39,40]. So far, there is no model that reports the generalized dimensions D_q or the singularity spectrum $f(\alpha)$ for the AE energies associated with the three PLC bands. Thus, our second objective is to examine if the calculated AE signals for the PLC bands [20,21] exhibit multifractality.

Towards this end, we follow the recently introduced framework for calculating AE for any plastic deforming situation [20,21]. We use the Rayleigh dissipation function to represent the energy dissipated during acoustic emission. The method involves setting up a discrete set of wave equations for the elastic strain with plastic strain rate as a source term. The plastic strain source term is itself calculated using the Ananthakrishna (AK) model for the PLC effect since the model predicts all the generic features of the PLC instability including the three band types [20,21]. This model also predicts Lüders-like bands. We demonstrate that the model AE energy bursts corresponding to the three types PLC bands and Lüders-like band predict both power-law distributions and multifractal spectra.

II. THEORETICAL FRAMEWORK FOR ACOUSTIC EMISSION DURING PLASTIC DEFORMATION

We briefly recall the theoretical framework developed for calculating AE in our previous papers [20,21]. The basic idea is that acoustic emission (transient elastic waves) is generated due to the abrupt motion of dislocations. In mathematical terms, this translates to setting up a wave equation for the elastic degrees of freedom with the plastic strain rate as a source term. At this point, the equation is general enough to be applicable to any plastic deformation since the plastic strain rate source term has no specific reference to the nature of plastic deformation. Therefore, to be applicable to a specific plastic deformation, we need to devise a suitable model that captures the characteristic features of the plastic deformation. In the present context, the minimum requirement is that the model should predict all the generic features of the PLC effect, including the three types of bands and the associated serrations. The AK model meets this requirement since the model captures most generic features of the PLC effect, including the band types [3,41–46]. The model also predicts the Lüders-like band.

A. Approach

As stated above, the abrupt motion of dislocations sets off an elastic disturbance, which then activates the dissipative forces that tend to oppose their growth so that mechanical equilibrium is restored. Then the dissipative energy [28,29,31,32,47] during AE is represented by the Rayleigh dissipation function $\mathcal{R}_{AE}$ [48] either in terms of the elastic strain ϵ_e or in terms of displacement field $u(y,t)$. Then we have

$$\mathcal{R}_{AE} = \frac{\eta}{2} \int \left[\frac{\partial \epsilon_e}{\partial t} \right]^2 dy = \frac{\eta}{2} \int \left[\frac{\partial \dot{u}(y,t)}{\partial y} \right]^2 dy, \quad (1)$$

where we have used the elastic strain defined by $\epsilon_e(y,t) = \frac{\partial u(y,t)}{\partial y}$. Here η the damping coefficient. Then, since $\mathcal{R}_{AE} \propto \dot{\epsilon}_e^2(y)$, we interpret $\mathcal{R}_{AE}$ as the acoustic energy dissipated during the abrupt motion of dislocations [28,29,31,32,47,49].

The total energy of a one-dimensional crystal is the sum of the kinetic energy, the potential energy, and the gradient potential energy [28,29,49]. The kinetic energy is given by $T = \frac{\rho}{2} \int [\frac{\partial u(y,t)}{\partial t}]^2 dy$, where ρ is the linear mass density. In our work we have chosen to use mass per unit volume instead of linear mass density so that the elastic constant μ appears naturally in the expression for the potential energy, given by $V_{\text{loc}} = \frac{\mu}{2} \int [\frac{\partial u(y,t)}{\partial y}]^2 dy$. (Note that the machine equation describing the constant strain rate condition contains the elastic constant.) The gradient potential energy is given by $V_{\text{grad}} = \frac{D}{4} \int [\frac{\partial^2 u(y,t)}{\partial y^2}]^2 dy$. Here D is the gradient energy coefficient. Then, using the Lagrangian $\mathcal{L} = T - V_{\text{loc}} - V_{\text{grad}}$ in the Lagrange equations of motion, we get

$$\rho \frac{\partial^2 u(y,t)}{\partial t^2} = \mu \frac{\partial^2 u(y,t)}{\partial y^2} + \eta \frac{\partial^2 \dot{u}(y,t)}{\partial y^2} - D \frac{\partial^4 u(y,t)}{\partial y^4}. \quad (2)$$

Noting that strain $\epsilon(y,t)$ is the natural variable used in plastic deformation, the wave equation in the strain variable is obtained by differentiating Eq. (2) with respect to y. Then we have

$$\rho \frac{\partial^2 \epsilon_e}{\partial t^2} = \mu \frac{\partial^2 \epsilon_e}{\partial y^2} + \eta \frac{\partial^2 \dot{\epsilon}_e}{\partial y^2} - D \frac{\partial^4 \epsilon_e}{\partial y^4}. \quad (3)$$

Equation (3) describes sound waves in the absence of dislocations. However, during plastic flow, since transient elastic waves are triggered by the abrupt motion of dislocations, we include the plastic strain rate $\dot{\epsilon}_p(y,t)$ as a source term in Eq. (3). Then the relevant inhomogeneous wave equation describing the AE process takes the form

$$\rho \frac{\partial^2 \epsilon_e}{\partial t^2} = \mu \frac{\partial^2 \epsilon_e}{\partial y^2} - \rho \frac{\partial^2 \epsilon_p}{\partial t^2} + \eta \frac{\partial^2 \dot{\epsilon}_e}{\partial y^2} - D \frac{\partial^4 \epsilon_e}{\partial y^4}. \quad (4)$$

Here $c = \sqrt{\mu/\rho}$ is the velocity of sound. Note that $\dot{\epsilon}_p(y,t)$ is a function of both space and time and hence contains full information of any possible heterogeneous character of the deformation. Clearly, the plastic strain rate source term needs to be *calculated independently* by setting up appropriate evolution equations for suitable types of dislocation densities for the desired plastic deformation. For the problem under consideration, we will use the AK model for the PLC effect.

Solution of Eq. (4) requires that we specify the initial and boundary conditions appropriate to the problem. Consider the commonly employed constant strain rate mode of deformation. This condition is enforced by fixing one end of the sample and applying a traction at the other end. However, it is important to ensure that the boundary conditions on Eq. (4) be consistent with those imposed on the evolution equations for the dislocation densities (subject to constant strain rate condition). However, the values of the dislocation densities at the boundaries are determined by physical considerations and therefore the plastic strain rate $\dot{\epsilon}_p(y,t)$ at the boundary points need not necessarily be consistent with those imposed on Eq. (4). (Note that the sum of the elastic and plastic strain rates should be equal to the imposed strain rate.) More importantly, in real samples, the machine stiffness gripping the ends of the

sample is higher than that for the sample. This condition is not easy to include in the continuous form of the wave equation, i.e., Eq. (4). On the other hand, this condition can be easily implemented in the equivalent discrete set of wave equations given in the Appendix (see also Ref. [21]). Such a discrete set of wave equations for $\epsilon_e(j,t)$, $j = 1, \ldots, N$, allows us to make a distinction between points within the sample and those at the boundary. Note that numerical solution of the evolution equations for the dislocation densities is obtained by solving them on a grid of N points corresponding to a sample length L by fixing one end and pulling the other end at a constant strain rate. Then the plastic strain rate computed for each spatial point can be directly used as source terms in the discrete set of N wave equations. The method also brings clarity to the boundary conditions. A brief outline of the discrete set of wave equations is given in the Appendix [Eqs. (A1)–(A5)]. For details see Ref. [21].

B. The Ananthakrishna model for the Portevin–Le Chatelier effect

Equation (4) [or Eqs. (A1)–(A5)] require that we supply the source term $\dot{\epsilon}_p(y,t)$ to compute the AE signals associated with the PLC bands. This then can be used for further statistical analysis. For the sake of completeness, we briefly recapitulate the AK model [3,41–43,45,46] for the PLC effect that was also used in Refs. [20,21] for calculating AE corresponding to the three PLC bands.

We begin with a brief summary of the salient features of the PLC effect. The PLC effect is characterized by three types of bands [3,4] and the associated stress serrations observed with increasing strain rate. At low applied strain rates $\dot{\epsilon}_a$, randomly nucleated static type C bands are seen with large-amplitude nearly regular serrations. With an increase in $\dot{\epsilon}_a$, hopping type B bands are seen that exhibit more irregular smaller serrations. Finally, at high $\dot{\epsilon}_a$, the continuously propagating type A bands are observed. The associated serration amplitudes are considerably smaller. These different types of PLC bands have been shown to represent distinct correlated states of dislocations in the bands [3,42–46].

We will use the AK model for the PLC effect since it predicts all the characteristic features of the phenomenon such as the existence of instability within a window of strain rates, the negative strain rate behavior [41,50], and the three types of band types C, B, and A [3,41–43,45,46]. The model also predicts several dynamical features reported in the analysis of the experimental time series such as the existence of chaotic stress drops [51], which has been subsequently verified [33,52,53]. Inclusion of spatial degrees of freedom automatically predicts the crossover dynamics from low-dimensional chaos to an infinite-dimensional power-law state of stress drops reported in the analysis of experimental stress-strain series [33,42–45,52,53]. In addition, the AK model also predicts Lüders-like bands [21].

The basic idea of the model is that all the qualitative features of the PLC effect emerge from a nonlinear interaction of a few collective degrees of freedom, namely, the densities of the mobile dislocations, immobile dislocations, and dislocations with a cloud of solute atoms, denoted, respectively, by $\rho_m(x,\tau)$, $\rho_{im}(x,\tau)$, and $\rho_c(x,\tau)$. The evolution

TABLE I. Parameter values used for the AK model for computation of the acoustic emission.

E^* (GPa)	σ_y (GPa)	α_m (s^{-1})	α_c (s^{-1})	v_0 (ms^{-1})	γ (s^{-1})	f	m	β (m^2 s^{-1})	Γ
48	0.2	0.8	0.08	10^{-7}	5×10^{-4}	1	3	5×10^{-14}	10^{12}

equations are

$$\frac{\partial \rho_m}{\partial t'} = -\beta \rho_m^2 - f\beta \rho_m \rho_{im} - \alpha_m \rho_m + \gamma \rho_{im}$$

$$+ \theta v_0 \left[\frac{\sigma_{\text{eff}}}{\sigma_y}\right]^m \rho_m + \frac{\Gamma \theta v_0}{\rho_{im}} \frac{\partial^2}{\partial x^2} \left[\frac{\sigma_{\text{eff}}}{\sigma_y}\right]^m \rho_m, \quad (5)$$

$$\frac{\partial \rho_{im}}{\partial t'} = \beta \rho_m^2 - \beta \rho_m \rho_{im} - \gamma \rho_{im} + \alpha_c \rho_c, \quad (6)$$

$$\frac{\partial \rho_c}{\partial t'} = \alpha_m \rho_m - \alpha_c \rho_c. \quad (7)$$

Equations (5)–(7) have been discussed in a number of earlier publications and the details can be found in Refs. [3,21,41–46,53]. For the sake of completeness, here we provide a brief description of each of the dislocation mechanisms.

The first term in Eq. (5) refers to the formation of dipoles. This term acts as a source term for ρ_{im}. The second term refers to the annihilation of a mobile dislocation with an immobile one. Here β has a dimension of the rate of the area swept by a dislocation. This is a common loss term to both ρ_m and ρ_{im}. The third term $\alpha_m \rho_m$ in Eq. (5) corresponds to solute atoms diffusing to mobile dislocations temporarily arrested at immobile (or forest) dislocations. Here α_m can be expressed in terms of the solute concentration c at the core of the dislocations, D_c is the diffusion constant of the solutes, and λ is an effective attractive length scale for the solute diffusion. Then $\alpha_m = D_c(T)c/\lambda^2$ (see [46]). The fourth term $\gamma \rho_{im}$ is the reactivation of the fraction of ρ_{im} that has been immobilized due to solute pinning (discussed below).

The loss term $\alpha_m \rho_m$ in Eq. (5) is a gain term for ρ_c. We consider those mobile dislocations that start acquiring solute atoms as dislocations with solute atoms ρ_c. As dislocations progressively acquire solute atoms at a rate α_c, they are eventually immobilized, at which point they are considered as ρ_{im}. Then the loss term $\alpha_c \rho_c$ in Eq. (7) is a source term for ρ_{im} in Eq. (6). (Note that $1/\alpha_c$ represents the aging time.) Thus, ρ_{im} includes dislocations that are pinned by solute atmosphere as well. Therefore, the loss term $\gamma \rho_{im}$ in Eq. (6) is considered to represent the unpinning of that fraction of ρ_{im} immobilized by the solute atoms.

The fifth term in Eq. (5) represents the rate of multiplication of dislocations due to cross slip given by $\theta v_m(\sigma_{\text{eff}})\rho_m = \theta v_0 [\sigma_{\text{eff}}/\sigma_y]^m \rho_m$, where m is a velocity exponent. Here $v_m(\sigma_{\text{eff}})$ is the mean velocity of mobile dislocations taken to have a power-law dependence on the effective stress $\sigma_{\text{eff}} = \sigma_a - h\rho_{im}^{1/2}$ [22]. In addition, σ_y is the yield stress and $h\rho_{im}^{1/2}$ the back stress. ($h = \alpha Gb$, where $\alpha \sim 0.3$, G is the shear modulus, and b is the magnitude of the Burgers vector.)

Several types of spatial couplings, such as solute diffusion to dislocations, double-cross-slip, long-range elastic interactions between dislocations, compatibility stresses between grains, the Bridgman factor (bending moments), and correlated

motion of dislocation glide due to long-range forces, have been proposed (see Ref. [3], pp. 130–133). In the context of theoretical modeling, even the long-range spatial couplings, such as the long-range elastic interaction between dislocations, the Bridgman factor, and correlated motion of dislocations, have been reduced to a diffusive type of coupling to the leading order [3]. In our model, the most natural spatial coupling [the sixth term in Eq. (5)] arises from the double-cross-slip process that allows dislocations to move into neighboring spatial elements. Note that the $1/\rho_{im}$ factor prevents the occurrence of cross slip into regions of high back stress. (See [3,45] for details of the derivations for different types of diffusive couplings.)

These equations are coupled to the machine equation that enforces the constant strain rate condition

$$\frac{d\sigma_a}{dt'} = E^* \left(\dot{\epsilon}_a - \frac{b}{L} \int_0^L v_0 \left[\frac{\sigma_{\text{eff}}}{\sigma_y}\right]^m \rho_m dx\right)$$

$$= E^*[\dot{\epsilon}_a - \dot{\epsilon}_p(t')]. \quad (8)$$

Here E^* is the effective modulus of the machine and the sample and L is the length of the sample.

Equations (5)–(8) are solved by using an adaptive step size differential equation solver (ode15s MATLAB solver). The model parameters fall into two types, one experimental and the other theoretical. In our approach, we can adopt the experimental parameters. Theoretical parameters correspond to parameters associated with dislocation mechanisms used in the model. The instability domain for various parameters has been determined in a number of publications [3,21,41–46,53]. The parameters used for calculation of AE signals (adopted from Ref. [21]) are given in Table I.

III. POWER-LAW STATISTICS FOR THE ACOUSTIC ENERGY DURING JERKY FLOW

As stated in the Introduction, the discrete set of wave equations for $\epsilon_e(j,t)$, $j = 1, \dots, N$, given by Eqs. (A1)–(A5) provides the general framework for calculating the AE signals provided the plastic strain rate source term can be calculated. For the present case, $\dot{\epsilon}_p$ is calculated by using the AK model equations that reproduce all the generic features of the PLC effect. The underlying physical mechanism subsumed in the AK model is the collective pinning and unpinning of dislocation from solute clouds. Clearly, the unpinning mechanism acts as a source generating the AE signals.

The numerical steps adopted for computing AE signals is detailed in Ref. [21]. The first step is to solve Eqs. (5)–(8) on a grid of N points for the entire time interval and obtain $\dot{\epsilon}_p(k,t_i')$ using a fixed or variable time step $\delta t'$. The so-computed $\dot{\epsilon}_p(k,t_i')$ can then be used as a source term in the N discrete wave equations (A1)–(A5). However, noting that the discrete wave equations need to be integrated at much finer time steps, say, δt, we first obtain the corresponding interpolated values of $\dot{\epsilon}_p(k,t_i)$ at these time steps, which are then used to solve

Eqs. (A1)–(A5). This gives the elastic strain rate, which is used to compute the AE energy dissipated using Eq. (1).

It should be mentioned here that the above method of calculating AE is only approximate since we use the equilibrated value of stress (8) to obtain the plastic strain rate $\dot{\epsilon}_p(k,t')$. The method is akin to adiabatic schemes. However, it is possible to solve the AK model equations (5)–(7) together with Eqs. (A1)–(A5) to obtain the elastic strain and hence the instantaneous stress along with the plastic strain rate. The so-computed stress will in general be different from the equilibrated value used in the approximate scheme.

A. Nature of the acoustic emission signals accompanying the PLC bands

Recall that, in our framework, acoustic emission is triggered by the plastic strain rate source term. The latter carries the physical information about the abrupt motion of dislocations. It is therefore useful to briefly recall some results from our earlier work [46] on the nature of the stress serrations associated with the three band types and their correlations with the nature of AE patterns [21]. At low strain rates, the uncorrelated static type C bands are seen with nearly regular large-amplitude serrations. As $\dot{\epsilon}_a$ is increased we see the hopping type B bands. The serrations are more irregular and are also of smaller magnitude. One important feature predicted by the model relevant to the AE studies is the correlation between band propagation property and small-amplitude serrations (SASs) and its influence on the AE pattern. It was recently demonstrated that band propagation induces small-amplitude serrations that are bounded on both sides by large-amplitude stress drops [46]. The latter were found to be well correlated with the nucleation and stopping of the band. As we increase $\dot{\epsilon}_a$, the extent of propagation increases with a concomitant increase of the SASs. At high $\dot{\epsilon}_a$ (type A bands), occasional large-amplitude stress drops accompany the SASs, identified with the band reaching the boundaries. These features are consistent with experimental studies [54,55]. Another feature that is relevant for the AE studies is the fact that the mean stress level of these SASs increases or decreases, though this change is small.

Now consider the nature of the AE signals accompanying the three types of PLC bands. For the type C band, well separated AE bursts are seen in the strain rate region 3×10^{-6} s^{-1} $< \dot{\epsilon}_a < 1.5 \times 10^{-5}$ s^{-1} [21]. Further, the bursts of AE are well correlated with the stress drops. Figure 1(a) shows typical burst-type AE signals for $\dot{\epsilon}_a = 1.125 \times 10^{-5}$ s^{-1}. The inset shows a few successive well separated AE bursts. The amplitude of each burst exhibits an oscillatory exponential decay, which, however, is not visible on the scale of the inset, but becomes visible on a finer scale. These features are consistent with AE experiments for the type C bands [14,15].

With increasing $\dot{\epsilon}_a$, the AE bursts begin to overlap in the region of the partially propagating type B bands. A typical plot of the AE for $\dot{\epsilon}_a = 3 \times 10^{-5}$ s^{-1} is shown in Fig. 1(b). The overall structure of the AE pattern is similar to the voltage plot of experimental AE signals in Fig. 2 of Ref. [24]. As shown in Ref. [21], a careful analysis of the AE signals and stress serrations shows two features. First, the low-amplitude continuous AE signals are well correlated with the band propagation induced SASs. Second, the large-amplitude AE
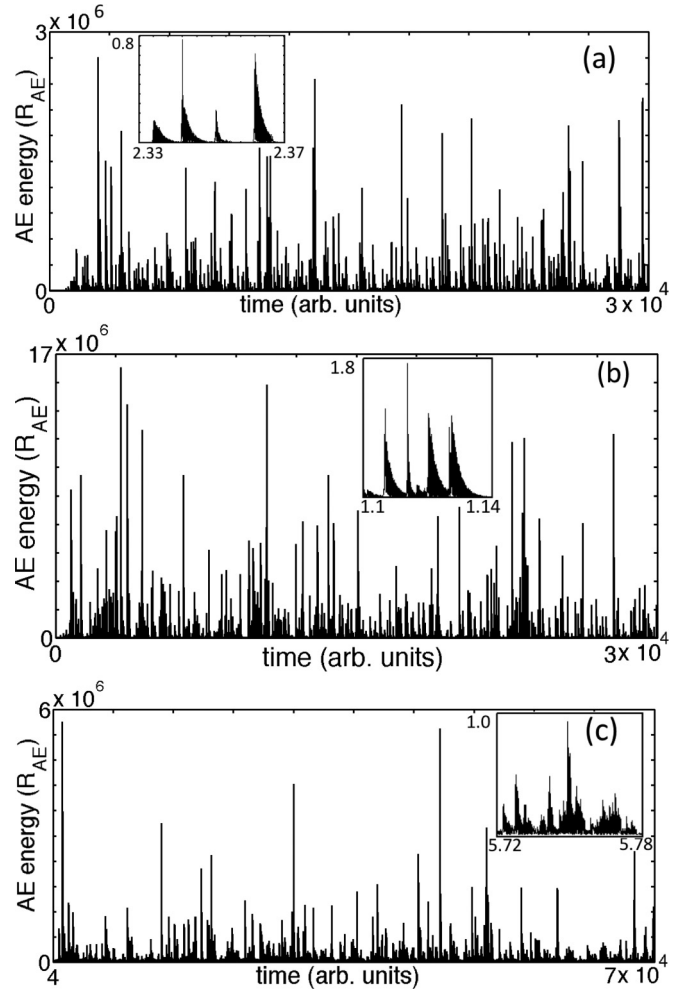

FIG. 1. Model acoustic energy R_{AE} associated with (a) the uncorrelated static type C bands for $\dot{\epsilon}_a = 1.125 \times 10^{-5}$ s^{-1}, (b) the partially propagating type B bands for $\dot{\epsilon}_a = 3.0 \times 10^{-5}$ s^{-1}, and (c) the fully propagating type A bands for $\dot{\epsilon}_a = 5.5 \times 10^{-5}$ s^{-1}. The inset in (a) shows the nonoverlapping nature of the bursts for the type C bands. The amplitude decreases in an oscillatory manner, not visible on this scale. The inset in (b) shows the increasing background AE level caused by SASs for the type B bands. The inset in (c) shows the increased level of background AE is due to the long stretches of SASs for the type A bands.

bursts (shown in the inset) are well correlated with the large-amplitude stress drops that are identified with the nucleation of new bands or stoppage of bands. This prediction is consistent with recent experimental studies on AE associated with the PLC bands [14,15].

At high $\dot{\epsilon}_a$ of the fully propagating type A bands, the nature of the AE pattern becomes nearly continuous, which again is due to the long stretch of SASs induced by type A bands propagating long distances. A typical AE pattern for $\dot{\epsilon}_a = 5.5 \times 10^{-5}$ s^{-1} is shown in Fig. 1(c). (It must be mentioned here that the small strain rate range over which the instability is seen is the limitation of the AK model as used here, which does not include the forest hardening term. This term was primarily ignored for mathematical convenience. However, inclusion of this term extends the instability range
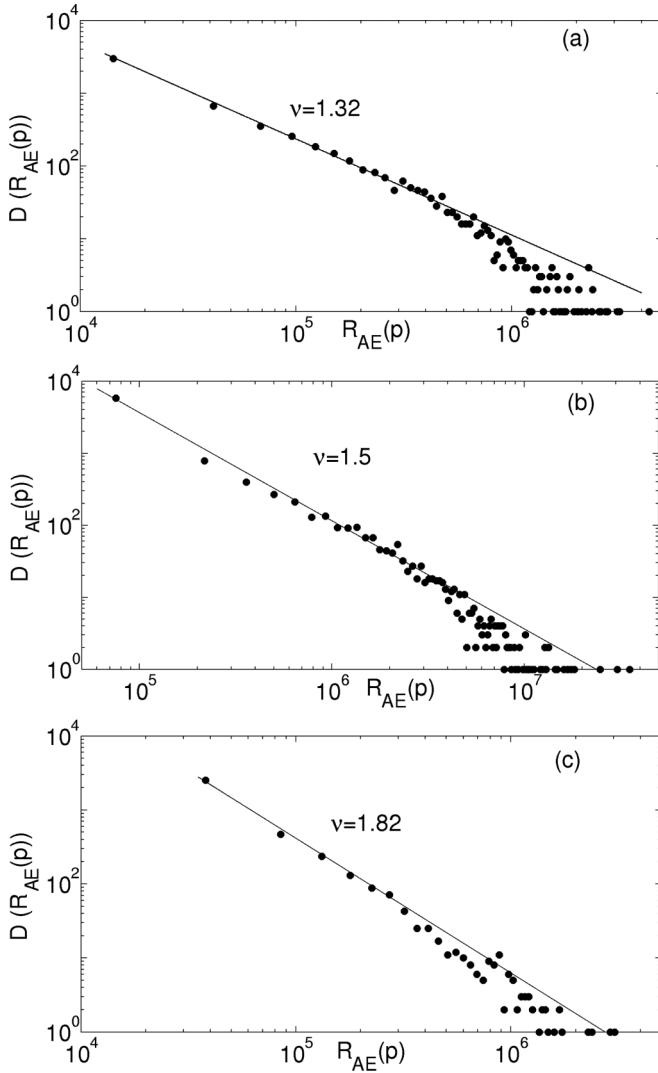
FIG. 2. Power-law distributions for the AE events $R_{AE}(p)$ for (a) the type C bands for $\dot{\epsilon}_a = 1.125 \times 10^{-5}$ s^{-1}, (b) the partially propagating type B band for $\dot{\epsilon}_a = 3.0 \times 10^{-5}$ s^{-1}, and (c) the type A band for $\dot{\epsilon}_a = 5.5 \times 10^{-5}$ s^{-1}.

to three orders in strain rate as in experiments [56].) As can be seen, the AE pattern has a nearly continuous background AE level with occasional relatively large bursts. The continuous background AE is illustrated in the inset. The high background level of the model AE signals corresponding to the type A band is also consistent with experiments [12–15]. In our earlier paper [21] we demonstrated that the relatively large AE bursts are correlated with the large-amplitude stress drops due to either nucleation or the band reaching the boundaries.

B. Power-law distributions of AE events associated with the PLC bands

Accumulation of the statistics of AE events requires identifying a segment of AE signals as an individual AE burst or an AE event. Recall that the AE signals corresponding to the type C bands consist of well separated AE bursts of varying peak amplitudes. In addition, we also find overlap of several successive AE bursts [see the inset of Fig. 1(a)]. Each of these

AE bursts shown in the inset of Fig. 1(a) decays in an oscillatory fashion. While the peak amplitude of all AE bursts decays in this manner, a few bursts may not relax fully due to the overlap with the next AE burst. In such cases, the amplitude of the AE signal first decreases and then increases to a new peak amplitude. When the strain rate is increased, the tendency for overlap of AE bursts increases, as is clear from the insets of Figs. 1(b) and 1(c). This feature helps us to define an individual AE burst or an AE event by the local peak amplitude of the burst. Using the local peak amplitude of each burst as the event size $R_{AE}(p)$, we have computed the distribution of the event sizes $D(R_{AE}(p))$. If the distribution $D(R_{AE}(p))$ follows a power law, then we have

$$D(R_{AE}(p)) \sim R_{AE}(p)^{-\nu}, \qquad (9)$$

where ν is the scaling exponent.

Here it is useful to briefly summarize the method used for accumulating the statistics of experimental AE bursts or events. Several factors influence the statistics of the AE event sizes. The first is the threshold imposed to identify what is regarded as an individual AE burst. (See Fig. 6 of Ref. [10].) The threshold, in particular, has a tendency to eliminate the AE signals that are smaller than the threshold value. In our calculation, the power-law distributions have been computed without any threshold. The second factor is that the exponent value depends on the region of the strain where the signal is recorded for the analysis. This is related to fact that the stress-strain curves exhibit hardening. In contrast, the model AE signals are recorded in the stationary region.

We have calculated the distribution of the magnitude of the AE events (AE energy bursts) $R_{AE}(p)$ associated with all three types of the PLC bands. A plot of $\ln D(R_{AE}(p))$ versus $\ln R_{AE}(p)$ for the type C bands is shown in Fig. 2(a). A scaling region of nearly two orders of magnitude in $R_{AE}(p)$ is clear and the exponent value is $\nu = 1.32$. At higher strain rates of partially propagating type B bands, the calculated distribution $D(R_{AE}(p))$ is shown in Fig. 2(b). The scaling regime is again nearly two orders in $R_{AE}(p)$ with an exponent value $\nu = 1.5$. In the fully propagating band A, we find a significantly larger proportion of small-amplitude AE events and a smaller number of large-amplitude AE events. The corresponding power-law distribution for $R_{AE}(p)$ is shown in Fig. 2(c). As can be seen, there is a reduced scaling region, a feature that is similar to experiments. The exponent value is $\nu = 1.8$. In all three cases, the model exponent values are considerably smaller than those reported by Lebyodkin and co-workers [10,19,24].

Finally, we consider analyzing the AE signals corresponding to another type of propagating band, namely, the Lüders band. It is well known that several alloys exhibiting the PLC effect also exhibit the Lüders band [14–16]. Since the AK model predicts the characteristic features of the three PLC bands, one can anticipate that the AK model should also predict a Lüders-like band. Indeed, the AK model also predicts a Lüders-like band following a yield drop. The corresponding AE pattern has been investigated [21]. Here we adopt the same parameters as used in Ref. [21] for calculating the AE signals associated with the Lüders-like band. The values are $\alpha_m = 1$ s^{-1}, $\alpha_c = 0.002$ s^{-1}, $\gamma = 5 \times 10^{-4}$ s^{-1}, $E^*/\sigma_y = 240$, $m = 10$, and $\dot{\epsilon}_a = 1.67 \times 10^{-6}$ s^{-1}. Figure 3(a) shows the stress-strain curve and associated AE signals. As can be
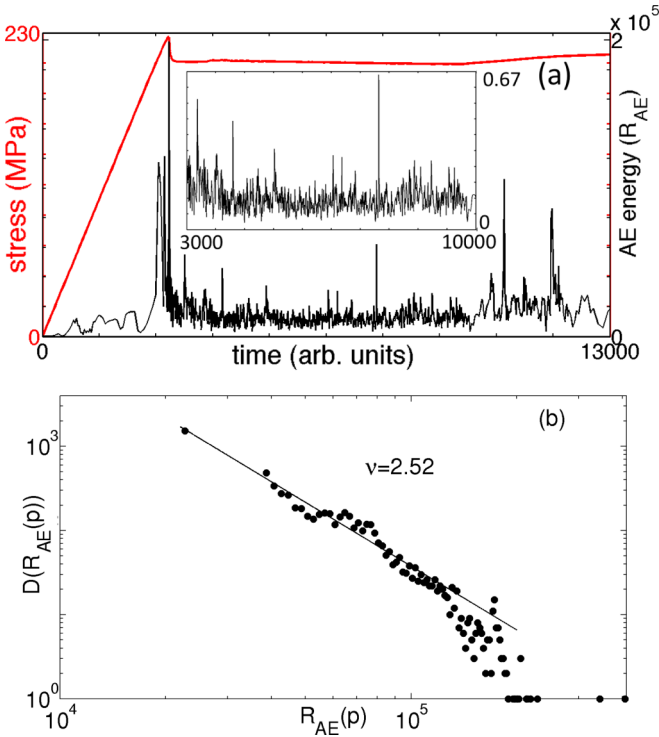
FIG. 3. (a) Model acoustic energy $R_{AE}(p)$ for the Lüders-like propagating band along with the stress-strain curve. (b) Corresponding power-law distribution for the AE signals $\dot{\epsilon}_a = 1.67 \times 10^{-6}$ s^{-1}.

seen, the AE pattern exhibits a peak corresponding to the yield drop, beyond which the AE amplitude decreases rapidly to an average AE level corresponding to the band propagation regime. The AE peak is due to the rapid multiplication of the dislocations from its initial low value. The steady level of AE activity during the band propagation can be identified with the production of new dislocation sources at the propagating front as it moves along the sample. The low-amplitude level of the AE signals is again attributable to the SASs induced by the propagating band [see the inset of Fig. 6(b) of Ref. [21]]. The nature of the AE pattern corresponding to the Lüders band predicted by the AK model is also consistent with experiments [14–16]. The calculated distribution of the AE bursts (sampled in the band propagation region) is shown in Fig. 3(b). As can be seen, the scaling region is only one order as for the type A band. The exponent $\nu \sim 2.51$. This value is significantly higher than the model exponent values for types C, B, and A, but is closer to the type A propagating band. The latter is understandable since both are propagating type bands that have a low level of stress fluctuations. However, there are no reports of a power-law distribution for the experimental AE signals in the case of the Lüders band for comparison with the model exponent value.

In summary, power-law distributions are predicted for the three PLC bands with exponent values increasing from 1.32 for the type C band to 1.82 for the type A band. Further, a power-law distribution for the Lüders band is also predicted by the model with an exponent 2.52. Thus. the power-law statistics of AE signals appear to be ubiquitous in PLC bands and the Lüders band.
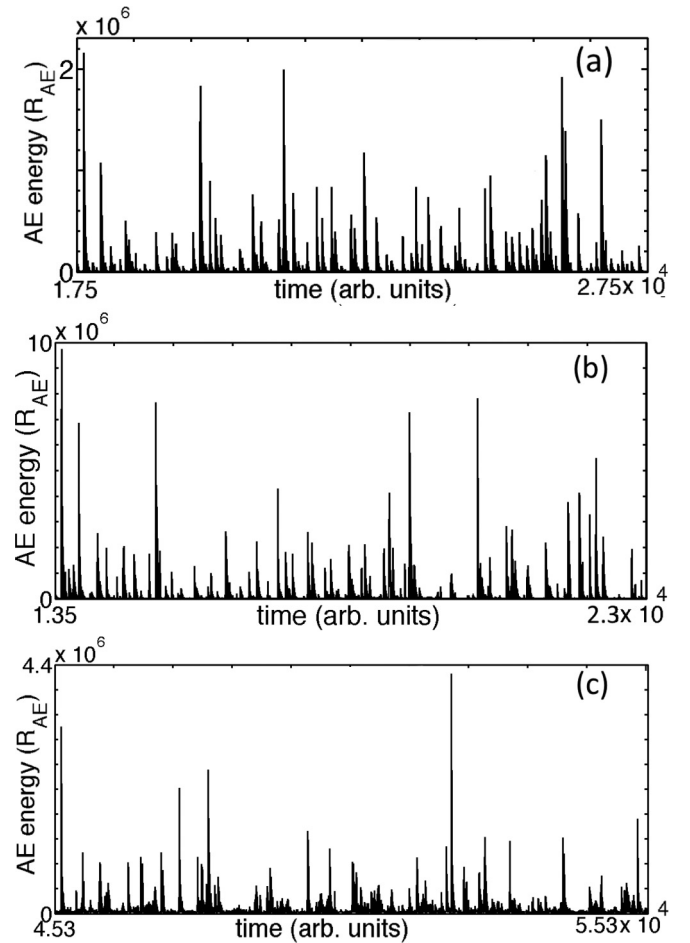

FIG. 4. Plots of respective subsegments of the AE signals shown in (a) Fig. 1(a) for the type C band, (b) Fig. 1(b) for the type B band, and (c) Fig. 1(c) for the type A band.

IV. MULTIFRACTAL ANALYSIS

Scale-invariant power-law distributions for events (of any kind) in a time series is the simplest statistical feature. Very often, such time series can possess much richer scaling properties than power-law distributions. For instance, the overall structure of the AE pattern corresponding to the three types of bands shown in Figs. 1(a)–1(c) is similar to the dissipated energy pattern in turbulent flows (compare these figures with Fig. 1 of Ref. [40]). The much richer scaling properties can be visualized by examining different segments of the AE time series on smaller scales. To illustrate this, consider the AE signals corresponding to $\dot{\epsilon}_a = 1.125 \times 10^{-5}$ s^{-1} shown in Fig. 1(a). The AE energy bursts do not appear to exhibit any obvious correlation between the successive bursts. However, the AE time series is not random either because the magnitudes of the AE bursts obey a scale-free power-law distribution, meaning that there is correlation at all scales. The time correlation is more subtle, which can be visualized by plotting a subsegment of the AE signals and comparing it with the whole. A plot of the subinterval $t = (1.75-2.75) \times 10^4$ is shown in Fig. 4(a). While a strict scale similarity to Fig. 1(a) is not seen, the overall structure appears to be statistically similar to the original AE segment. In fact, this kind of statistical scale

similarity is exhibited by any subsegment. This suggests that different segments have different scaling exponents. This kind of statistical scale similarity is also seen for the AE patterns corresponding to the type B and A bands. This is illustrated in the plots of subsegments of Figs. 1(b) and 1(c) shown in Figs. 4(b) and 4(c), respectively.

Such multiscale similarity of sets is known to lead to highly nonuniform probability distributions instead of a simple power-law distribution. Such nonuniform distributions require a continuum of scaling exponents for their characterization. The emergence of such nonuniform distributions has been attributed to the underlying nonlinear dynamical evolution of the system as established in a number of physical situations such as turbulence, distribution of growth probabilities of a diffusion-limited aggregate [39,40,57–59], stress drop magnitudes in type A PLC bands [33,34,53], and AE energies associated with type C, B, and A bands [19]. Then statistical characterization of the self-similar (fractal) properties is carried out in terms of the measures associated with the nonuniform distribution. This is the basis of multifractal formalism. The characterization is done in terms of the commonly used generalized Rényi dimensions D_q parametrized by q or in terms of the singularity spectrum $f(\alpha)$ of singularity strengths α associated with the nonuniform distribution [38–40,57,58]. A direct way of calculating the singularity spectrum was introduced as an alternate way of characterizing nonuniform distributions [40].

Generalized dimension and singularity spectrum

As in many physical systems, in our case also, the AE signals occur in time and therefore the support of the measure is the real line. Then a length L of the time series can be covered by N segments of time interval δt and we have $N\delta t = L$. Let R_{AEi} be the acoustic energy dissipated in the ith interval. Then the probability $P_i(\delta t)$ of the acoustic energy dissipated in the ith interval is given by $P_i(\delta t) = R_{AEi}/\sum_i^N R_{AEi}$. The generalized dimension D_q is defined by

$$D_q = \frac{1}{q-1} \lim_{\delta t \to 0} \frac{\ln \sum_i P_i^q}{\ln \delta t}. \tag{10}$$

Here q is a real number taken as a parameter. The structure of Eq. (10) provides a straightforward physical interpretation. The positive q's accentuate the denser regions (high probabilities) of the nonuniform distribution, while the negative q's accentuate the rarer regions (small probabilities).

Alternately, multifractals can be defined as interwoven sets with fractal (Hausdorff) dimensions $f(\alpha)$ having a singularity strength α. In this formalism, the probability of the ith box is taken to scale as $P_i(\delta t) \sim \delta t^{-\alpha_i}$. The number of boxes $N(\alpha)$ with singularity strength between α and $d\alpha$ is given by $N(\alpha) \sim \delta t^{-f(\alpha)}$. The singularity spectrum $f(\alpha)$ of a multifractal is related to D_q through a Legendre transformation [provided $f(\alpha)$ and D_q is a smooth function of α and q]. Then

$$(q-1)D_q = q\alpha - f(\alpha), \quad \alpha = \frac{d}{dq}(q-1)D_q. \tag{11}$$

However, obtaining the $f(\alpha)$ spectrum using the computed D_q values requires evaluation of the derivatives. This can lead to uncontrolled errors, particularly in the analysis of experimental data. In view of this, a direct computation of
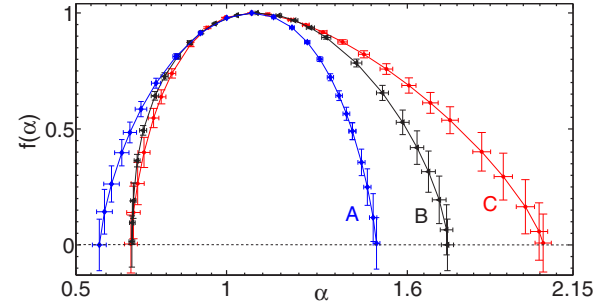

FIG. 5. Multifractal spectrum $f(\alpha)$ associated with the AE signals accompanying the type C, B, and A bands for $\dot{\epsilon}_a = 1.125, 3.0,$ and 5.5×10^{-5} s^{-1}, respectively.

$f(\alpha)$ has been suggested [40]. The method involves defining normalized measures $\mu_i(\delta t, q)$ by

$$\mu_i(\delta t, q) = \frac{P_i^q}{\sum_j P_j^q} \tag{12}$$

in terms of the probabilities P_i defined earlier. Using $\mu_i(\delta t, q)$ and $P_i(\delta t)$, we can directly calculate the multifractal spectrum $f(\alpha)$ as a function of α using [40]

$$\alpha = \lim_{\delta t \to 0} \frac{\sum_i \mu_i(\delta t, q) \ln P_i(\delta t)}{\ln \delta t} \tag{13}$$

and

$$f(\alpha) = \lim_{\delta t \to 0} \frac{\sum_i \mu_i(\delta t, q) \ln \mu_i(\delta t, q)}{\ln \delta t}. \tag{14}$$

We use the direct method of computing the $f(\alpha)$ spectrum. Numerically, the multifractal spectrum for a given data set is calculated by plotting $\ln \sum \mu_i \ln \mu_i$ and $\ln \sum \mu_i \ln P_i$ as a function of $\ln \delta t$ to obtain the respective slopes for each q. The slope of $\ln \sum \mu_i \ln \mu_i$ versus $\ln \delta t$ gives $f(q)$, while $\ln \sum \mu_i \ln P_i$ versus $\ln \delta t$ gives $\alpha(q)$. In general, the log-log plots begin to exhibit scatter for increasing positive and negative q values. This is due to the poor statistics corresponding to small δt bins. For this reason, a fit is obtained by considering those bins with reasonable statistics (i.e., bins of larger δt). Such a scatter for large positive and negative values of q is common to multifractal calculations. (See plots of $\sum \mu_i \ln P_i$ in Fig. 6 of Ref. [40].) In our calculation, the range over which $\alpha(p)$ and $f(p)$ are calculated is at least two orders of magnitude in δt. While we had no difficulty in getting good fits to the slopes even for large q, the error bars increase for large q, particularly for $f(q)$, as will be clear below.

We have computed the singularity spectrum $f(\alpha)$ corresponding to the AE spectra [shown in Figs. 1(a)–1(c)] corresponding to type C, B, and A bands. Figure 5 shows the $f(\alpha)$ spectra corresponding to the AE signals associated with the three PLC bands. It is clear that the maximum value of $f(\alpha)$ is unity in all three cases, as it should be for a set whose support is the real line. Several features are evident. First, the $f(\alpha)$ spectrum of the AE signals associated with the type C band is skewed to the right with significantly larger error bars for higher values of α. This is due to a higher proportion of large-amplitude AE bursts compared to the type B and A bands. Second, the width of the multifractal spectrum defined by
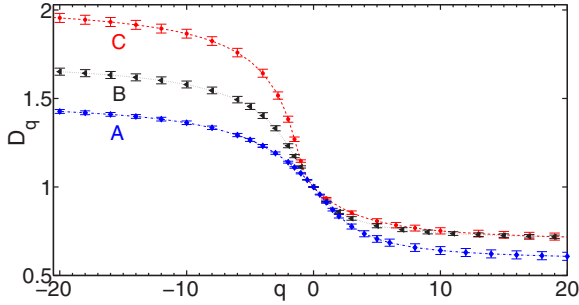
FIG. 6. Generalized dimensions for the AE events associated with the type C, B, and A bands for $\dot{\epsilon}_a = 1.125$, 3.0 and 5.5×10^{-5} s^{-1}.

$\theta = \alpha_{max} - \alpha_{min}$, with α_{min} and α_{max} referring to the extreme values of α, is maximum for the type C AE signals, decreasing to a minimum for the AE signals corresponding to the type A band. The third feature is that α_{min} is nearly the same for all three band types. This feature is also understandable since, unlike the probability of large-amplitude AE bursts being quite different, the probabilities for small-amplitude AE signals are not significantly different.

The generalized dimension corresponding the AE signals for the three types of bands can now be easily calculated by using Eq. (11). The corresponding D_q's as a function of q are shown in Fig. 6. Again, the range of D_q is largest for the type C band, while it is lowest for the type A band.

We have also calculated the multifractal spectrum for the Lüders-like band. This is shown in Fig. 7. The range of $\theta = \alpha_{max} - \alpha_{min}$ is similar to that of the type A band, as expected.

V. DISCUSSION AND CONCLUSIONS

The present work is motivated by the lack of any model for the statistical characterization of the AE signals accompanying the three band types in the PLC effect [10,23,24]. In particular, our study reports both power-law distributions and multifractal spectra for the AE energies. Two types of statistical characterization of the model AE signals have been attempted. The first one is to examine if the model AE signals follow power-law distributions for the AE energies associated with the C, B, and A PLC bands. We have also carried out a similar study for the Lüders-type band. The second type of statistical analysis is the possibility of multifractal spectra for the AE energies associated with the PLC and Lüders bands. Within
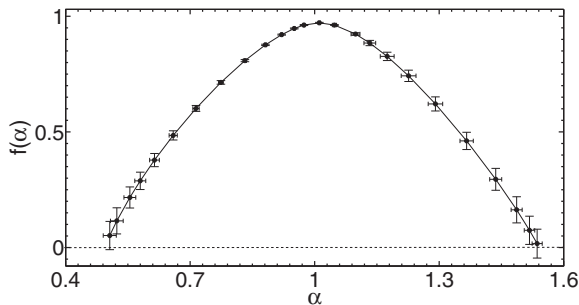

FIG. 7. Multifractal spectrum $f(\alpha)$ for the Lüders-like propagating band for $\dot{\epsilon}_a = 1.67 \times 10^{-6}$ s^{-1}.

our framework, the AE signals are calculated as solutions to the discrete set of wave equations with a plastic strain rate as a source term. The latter is computed using the AK model for the PLC effect since the model predicts the three PLC bands and the Lüders-like propagating band.

The present study demonstrates that the statistical analysis of the peak amplitudes of the model AE bursts associated with the three PLC bands exhibits power-law distributions consistent with experiments [10,23,24]. We have also verified that the AE bursts corresponding to the Lüders-like band also follow a power-law distribution. Since there are no reports of the statistical analysis of the AE events for this case, it would be interesting to verify this prediction. However, the model exponent values corresponding the three PLC bands are significantly smaller than the reported values. Further, while the reported exponent values decrease as we move from type C to the type A bands, our results show the opposite trend. This mismatch requires a critical examination.

In this context, it must be stated that a comparison between the reported exponent values and the model exponent values is not straightforward because the former depends on several experimental variables. Similarly, several factors such as modeling the AE signals and modeling the PLC bands contribute to the computed exponent values. From the experimental side, there are several factors that affect the exponent such as preparation of the samples, the nature of the sample, sample history, for instance, how long the samples are aged, sample-to-sample variation, testing conditions, etc. From the modeling side, the one-dimensional nature of the wave equation used for calculating the AE signals and the calculation of the plastic strain rate source term clearly affects the exponent values. In addition, any effort in modeling such a complex spatiotemporal phenomenon as the PLC effect can only constitute idealization and therefore can be expected to contribute. Clearly, the AK model is no exception, even though the model predicts all the characteristic features of the PLC effect mentioned in Sec. III A, including the band types.

While the above factors could be contributing to the smaller values of the model exponents compared to the previously reported values, the increasing trend of the model exponents as we progress from type C to A bands needs a critical examination, particularly in view of the fact that the AK model predicts most generic features of the PLC effect. Here we argue that this trend appears to be consistent with the physical (mathematical) mechanism underlying acoustic emission used in our approach together with the dynamic strain aging mechanism specific to the PLC effect subsumed in the AK model. To see this, we first note that the model AE signals are computed by using the well established mechanism that acoustic emission is triggered by the release of the stored energy. The latter information is contained in the plastic strain rate and is computed from the AK model. Now we examine how the aging kinetics of dislocations determines the nature of the AE pattern. For instance, the type C serrations are the result of unpinning of fully aged dislocations. This means that the unpinning stress is high. Thus, once unpinned, the kinetic energy imparted to the lattice is high and therefore the corresponding AE bursts are generally large. For higher strain rates where the type B and A bands are seen, there is less time to complete the aging process and therefore lower stress is required to unpin dislocations compared to the

type C bands. Consequently, the transferred kinetic energy to the lattice is lower, leading to a larger proportion of lower-level AE bursts. At high strain rates of the type A bands, there is even less time for the aging process to occur and therefore even smaller stress is required to unpin dislocations. Therefore, a large proportion of the AE signals should be expected to be small-amplitude signals and thus significantly fewer larger AE bursts. Indeed, we have recently demonstrated [21] that in general the AE bursts associated with type C are of large amplitude and well separated. In contrast, for the type B bands, fluctuations in stress level are low during propagation with occasional large stress drops occurring during nucleation of a band or when the band stops [46]. In the type A band case, due to the band propagating over large distances, the amplitude of the stress serrations is small with relatively large stress drops seen only when the band reaches the sample boundaries. Then, using the fact that AE signals are proportional to unpinning stress, the relative proportion of large-amplitude AE bursts is higher for the type C than for the type B or type A. This has been demonstrated in Ref. [21]. On the other hand, considering the fact that a relatively larger proportion of SASs are seen for the type B and even more for the A bands, we expect a larger proportion of small-amplitude AE bursts for the type B and A bands compared to the type C bands. This implies that the exponent corresponding to the type C band AE events should be lowest, and increasing for type B and then for the type A bands. This is precisely the trend exhibited by the model exponents.

In view of the above discussion, we look for other possible sources of discrepancy between our model results and the experimental results. For instance, experimental stress-strain curves always exhibit considerable hardening. The exponent value corresponding to the AE signals recorded in the regions of increasing strains increase from 2.5 approaching a saturation level of 3.0. Noting that signals can be considered as stationary only when the stress-strain curve reaches the saturation regime, the AE time series itself is nonstationary during the hardening region. This raises questions about the possible influence of nonstationarity on the exponent values. This issue, however, has so far not been investigated in any context. Thus, the reported exponent values corresponding to the hardening regime are subject to this criticism. This is not applicable to the exponent value corresponding to stationary regime ($\sim$3). Noting that the version of AK model used here exhibits a low level of hardening, even if one wishes to examine the dependence on strain, the generalized AK model that includes a work hardening trend is more appropriate [56]. In contrast, the model AE statistics has been compiled in the stationary state. The model exponent values are however significantly low.

On the other hand, the exponent values are sensitive to the threshold value used for recording an AE burst as a single event. In experiments, a stretch of an AE signal is regarded as an individual AE event when the amplitude of the signal stays above a chosen threshold value. Lebyodkin *et al.* [23] reported that increasing the threshold by a factor of 3.3 decreases the exponent from 2.54 to 2.1 for the type C band, with a concomitant decrease in the scaling region (see Fig. 6 of Ref. [10]). Further, a higher threshold has a tendency to eliminate small-amplitude AE bursts, thereby decreasing the exponent value. Indeed, we have verified that increasing the

threshold value of the recording, the model exponent value decreases along with the scaling regime. Furthermore, for higher strain rates, smaller events dominate and two successive peak heights that are close to each other will be regarded as one when the threshold is higher. Thus, at high strain rates small events are undersampled. This suggests that the exponent values for the type B and A bands should be expected to be higher than what is reported. This means that using a lower threshold can reverse the decreasing trend of the exponent values for the experimental AE signals as we increase strain rates. However, this depends on the capability of the experimental setup.

On the modeling side, other than the influence of idealizations discussed above, one obvious idealization that affects the calculated AE signals is that the solutions of the model equations (both the wave equation and the AK model) have been obtained in one space dimension, while real samples are three dimensional. One other possible influence on the computed exponent values is the numerical accuracy of computation of the solutions of the model differential equations. We have specifically investigated this aspect by increasing the accuracy of computation by one order. We find that the exponent value increases, though not significantly. Another factor that could affect the model AE statistics is the algorithm employed for computing the AE signals. Recall that AE is calculated using the plastic strain rate computed using the AK model. However, the computed plastic strain rate $\dot{\epsilon}_p$ has been obtained using Eq. (8), which assumes stress equilibration. This was done for the sake of convenience of computation (and the procedure akin to adiabatic methods). The framework itself is more general than the methodology followed here for computing $\dot{\epsilon}_p$. However, the stress equilibration constraint can easily be lifted by using the instantaneous stress that can be obtained from the elastic strain calculated from the wave equation. This again can affect the exponent value.

In view of the above discussion, it is unrealistic to expect a match of model exponent values with that reported for the experimental AE energies. On the other hand, while factors that affect the exponents in experiments have a tendency to reverse the increasing trend of the exponent values, the factors contributing from the modeling efforts have a tendency to reverse the increasing trend of model exponents. Again, it is difficult to make a quantitative assessment of how the experimental and theoretical factors affect the trends of the exponents. The question whether the exponent values should increase with strain rate or not remains unresolved.

We have also computed the multifractal spectra for the AE signals associated with the three PLC bands and the Lüders-like propagating band. The multifractal spectra have been computed using the direct method of computing the $f(\alpha)$ spectrum [40]. This circumvents using the Legendre transformation of $\tau(q)$ to obtain the $D(q)$, a procedure that often leads to uncontrolled errors. The direct method used here is better suited for analyzing numerical data. The computed $f(\alpha)$ spectra for the three PLC bands are all smooth. The width of the multifractal spectrum decreases from a maximum value for the type C band to a minimum for the type A bands. The corresponding D_q's also show the same trend. A comparison with the results reported by Lebyodkin and co-workers [18,19] is not possible since the reported $f(\alpha)$ spectra are not in the

stationary state. We have also calculated the $f(\alpha)$ spectrum for the Lüders-like band. There are no reports of the $f(\alpha)$ spectrum for the Lüders band for comparison.

In summary, a significant characteristic feature, namely, the power-law distributions for the AE bursts for all three types of PLC band, is predicted by our approach. However, the model exponent values and their increasing trend with increasing strain rates does not match with the reported values and trend. The possible causes contributing to these two differences discussed in detail show that a comparison between model exponent values and those for the experimental AE signals is not meaningful because the reported exponent values depend on several experimental variables as well as those in modeling a complex spatiotemporal phenomenon such as the PLC effect. A power-law distribution for the model AE bursts is also obeyed for the Lüders-like band. The approach also correctly captures the reported multifractal nature of the AE spectra associated with the PLC bands and Lüders band.

APPENDIX

In this Appendix we briefly recall the discrete wave equations used for computing acoustic emission. (See Ref. [21] for details.) To do this, consider a spring-block system of N points of mass m coupled to each other through near-neighbor springs pulled at a constant strain rate by holding one end of the sample fixed and pulling the other. The fact that the ends of the sample are gripped by the machine translates to choosing the force constant k_m for the boundary points to be much larger than the spring constant k_s for the interior points. Then the kinetic energy T, the local potential energy V_{loc}, the gradient potential energy V_{grad}, and the dissipated acoustic energy R_{AE} [Eq. (1)] are written down easily in terms of the displacement $u(i,t)$ defined at each site. It is then straightforward to set up the corresponding set of wave equations. Taking the spatial derivative of these equations, the discrete set of wave equations in terms of the elastic strain variables $\epsilon_e(i,t)$, which include the plastic strain rate source terms $\dot{\epsilon}_p(i,t)$, takes the form

$$\ddot{\epsilon}_e(1) = 0.0, \tag{A1}$$

$$\ddot{\epsilon}_e(2) = -\frac{c^2}{a^2}\left[\{\epsilon_e(2) - \epsilon_e(3)\} + \frac{k_m}{k_s}\epsilon_e(2)\right] - \frac{\partial \dot{\epsilon}_p(2,t)}{\partial t}$$
$$- \frac{\eta'}{a^2\rho}[\dot{\epsilon}_e(2) - \dot{\epsilon}_e(3)] + \frac{D'}{a^4\rho}[\epsilon_e(4) + \epsilon_e(2) - 2\epsilon_e(3)], \tag{A2}$$

$$\ddot{\epsilon}_e(3) = \frac{c^2}{a^2}[\epsilon_e(4) + \epsilon_e(2) - 2\epsilon_e(3)] - \frac{\partial \dot{\epsilon}_p(3,t)}{\partial t}$$
$$+ \frac{\eta'}{a^2\rho}\{\dot{\epsilon}_e(4) + \dot{\epsilon}_e(2) - 2\dot{\epsilon}_e(3)\}$$
$$- \frac{D'}{a^4\rho}\{\epsilon_e(5) - 4\epsilon_e(4) + 5\epsilon_e(3) - 2\epsilon_e(2)\}, \tag{A3}$$

$$\ddot{\epsilon}_e(i) = \frac{c^2}{a^2}\{\epsilon_e(i+1) - 2\epsilon_e(i) + \epsilon_e(i-1)\} - \frac{\partial \dot{\epsilon}_p(i,t)}{\partial t}$$
$$+ \frac{\eta'}{a^2\rho}\{\dot{\epsilon}_e(i+1) - 2\dot{\epsilon}_e(i) + \dot{\epsilon}_e(i-1)\}$$
$$- \frac{D'}{a^4\rho}[\epsilon_e(i+2) - 4\epsilon_e(i+1) + 6\epsilon_e(i)$$
$$- 4\epsilon_e(i-1) + \epsilon_e(i-2)], \tag{A4}$$

$$\ddot{\epsilon}_e(N-1) = -\frac{c^2}{a^2}\left[\{\epsilon_e(N-1) - \epsilon_e(N-2)\}\right.$$
$$\left. - \frac{k_m}{k_s}\{\epsilon_e(N) - \epsilon_e(N-1)\}\right] - \frac{\partial \dot{\epsilon}_p(N-1,t)}{\partial t}$$
$$+ \frac{\eta'}{a^2\rho}[\dot{\epsilon}_e(N) + \dot{\epsilon}_e(N-2) - 2\dot{\epsilon}_e(N-1)]$$
$$- \frac{D'}{a^4\rho}[\epsilon_e(N-3) - 4\epsilon_e(N-2)$$
$$+ 5\epsilon_e(N-1) - 2\epsilon_e(N)]. \tag{A5}$$

Equation (A4) is valid for $i = 4, \ldots, N-1$. The mass density $\rho = m/a^3$ and the velocity of sound is $c = \sqrt{\mu/\rho}$ [see Eq. (4)] with $\mu = k_s/a$, $\eta' = \eta/a$, and $D' = Da$. The plastic strain rate $\dot{\epsilon}_p$ obtained from the AK model (5)–(8) is used as a source term in Eqs. (A1)–(A5). Equations (A1)–(A5) are solved by using a differential equation solver (ode15s MATLAB solver) with appropriate initial and boundary conditions. The initial conditions are

$$\epsilon_e(1,0) = 0,$$
$$\epsilon_e(i,0) = 0 + \xi \times \epsilon_r, \quad i = 2, \ldots, N-1, \tag{A6}$$

where ϵ_r ($\sim 10^{-7}$) represents the strain due to inherent defects in the sample and ξ is a random number in the interval $-\frac{1}{2} < \xi < \frac{1}{2}$. The left-hand side of the sample is fixed and right-hand side is pulled at a constant strain rate $\dot{\epsilon}_a$. So the boundary conditions for the wave equation are

$$\epsilon_e(1,t) = 0, \quad \epsilon_e(N,t) = \dot{\epsilon}_a t, \quad t > 0. \tag{A7}$$

The time step required for integrating Eqs. (A1)–(A5) needs to be substantially smaller than that for the AK model. This requires that the time variables in Eqs. (A1)–(A5) and Eqs. (5)–(8) are matched correctly. [Interpolated values for $\epsilon_p(k,t')$ are used as input in Eqs. (A1)–(A5).] (For details see Ref. [21].)

[1] M. D. Uchic, P. A. Shade, and D. M. Dimiduk, Annu. Rev. Mater. Res. **39**, 361 (2009).

[2] M. Zaiser, J. Schwerdtfeger, A. S. Schneider, C. P. Frick, B. G. Clark, P. A. Gruber, and E. Arzt, Philos. Mag. **88**, 3861 (2008).

[3] G. Ananthakrishna, Phys. Rep. **440**, 113 (2007).

[4] A. Yilmaz, Sci. Technol. Adv. Mater. **12**, 063001 (2011).

[5] H. Dunegan and D. Harris, Ultrasonics **7**, 160 (1969).

[6] Z. Han, H. Luo, and H. Wang, Mater. Sci. Eng. A **528**, 4372 (2011).

[7] J. Weiss and J. R. Grasso, J. Phys. Chem. B **101**, 6113 (1997).

[8] J. Weiss, T. Richeton, F. Louchet, F. Chmelík, P. Dobron, D. Entemeyer, M. Lebyodkin, T. Lebedkina, C. Fressengeas, and R. J. McDonald, Phys. Rev. B **76**, 224110 (2007).

[9] M. C. Miguel, A. Vespignani, S. Zapperi, J. Weiss, and J. R. Grasso, Nature (London) **410**, 667 (2001).

[10] M. A. Lebyodkin, I. V. Shashkov, T. A. Lebedkina, K. Mathis, P. Dobron, and F. Chmelík, Phys. Rev. E **88**, 042402 (2013).

[11] D. R. James and S. H. Carpenter, J. Appl. Phys. **42**, 4685 (1971).

[12] C. H. Caceres and Rodriguez, Acta Metall. **35**, 2851 (1987).

[13] F. Zeides and J. Roman, Scr. Metall. Mater. **24**, 1919 (1990).

[14] F. Chmelík, A. Ziegenbein, H. Neuhaüser, and P. Lukáč, Mater. Sci. Eng. A **324**, 200 (2002).

[15] F. Chmelík, F. B. Klose, H. Dierke, J. Šachl, H. Neuhäuser, and P. Lukáč, Mater. Sci. Eng. A **462**, 53 (2007).

[16] T. V. Murav'ev and L. B. Zuev, Technol. Phys. **53**, 1094 (2008).

[17] A. A. Shibkov and A. E. Zolotov, Crystalogra. Rep. **56**, 141 (2011).

[18] M. A. Lebyodkin, T. A. Lebedkina, F. Chmelík, T. T. Lamark, Y. Estrin, C. Fressengeas, and J. Weiss, Phys. Rev. B **79**, 174114 (2009).

[19] M. A. Lebyodkin, N. P. Kobelev, Y. Bougherira, D. Entemeyer, C. Fressengeas, T. A. Lebedkina, and I. V. Shashkov, Acta Mater. **60**, 844 (2012).

[20] J. Kumar and G. Ananthakrishna, Phys. Rev. Lett. **106**, 106001 (2011).

[21] J. Kumar, R. Sarmah, and G. Ananthakrishna, Phys. Rev. B **92**, 144109 (2015).

[22] H. Neuhäuser, in *Dislocations in Solids*, edited by F. R. N. Nabarro (North-Holland, Amsterdam, 1983), Vol. 6.

[23] M. A. Lebyodkin, N. P. Kobelev, Y. Bougherira, D. Entemeyer, C. Fressengeas, V. S. Gornakov, T. A. Lebedkina, and I. V. Shashkov, Acta Mater. **60**, 3729 (2012).

[24] I. V. Shashkov, M. A. Lebyodkin, and T. A. Lebedkina, Acta Mater. **60**, 6842 (2012).

[25] P. Diodati, F. Marchesoni, and S. Piazza, Phys. Rev. Lett. **67**, 2239 (1991).

[26] A. Petri, G. Paparo, A. Vespignani, A. Alippi, and M. Costantini, Phys. Rev. Lett. **73**, 3423 (1994).

[27] E. Vives, I. Ràfols, L. Mañosa, J. Ortín, and A. Planes, Phys. Rev. B **52**, 12644 (1995).

[28] R. Ahluwalia and G. Ananthakrishna, Phys. Rev. Lett. **86**, 4076 (2001).

[29] S. Sreekala and G. Ananthakrishna, Phys. Rev. Lett. **90**, 135501 (2003).

[30] M. Ciccotti, B. Giorgini, D. Villet, and M. Barquins, Int. J. Adhes. Adhes. **24**, 143 (2004).

[31] R. De and G. Ananthakrishna, Phys. Rev. Lett. **97**, 165503 (2006).

[32] J. Kumar, R. De, and G. Ananthakrishna, Phys. Rev. E **78**, 066119 (2008).

[33] G. Ananthakrishna, S. J. Noronha, C. Fressengeas, and L. P. Kubin, Phys. Rev. E **60**, 5455 (1999).

[34] M. A. Lebyodkin, Y. Brechet, Y. Estrin, and L. P. Kubin, Phys. Rev. Lett. **74**, 4758 (1995).

[35] M. S. Bharathi, M. A. Lebyodkin, C. Fressengeas, and L. P. Kubin, Acta Mater. **50**, 2813 (2002).

[36] F. F. Csikor, C. Motz, D. Weygand, M. Zaiser, and S. Zapperi, Sience **318**, 251 (2007).

[37] P. Bak, C. Tang, and K. Wiesenfeld, Phys. Rev. Lett. **59**, 381 (1987); Phys. Rev. A **38**, 364 (1988).

[38] A. Rényi, *Probability Theory* (North-Holland, Amsterdam, 1970).

[39] T. C. Halsey, M. H. Jensen, L. P. Kadanoff, I. Procaccia, and B. I. Shraiman, Phys. Rev. A **33**, 1141 (1986).

[40] A. B. Chhabra and R. V. Jensen, Phys. Rev. Lett. **62**, 1327 (1989); A. B. Chhabra, C. Meneveau, R. V. Jensen, and K. R. Sreenivasan, Phys. Rev. A **40**, 5284 (1989).

[41] G. Ananthakrishna and M. C. Valsakumar, J. Phys. D **15**, L171 (1982).

[42] M. S. Bharathi and G. Ananthakrishna, Europhys. Lett. **60**, 234 (2002).

[43] M. S. Bharathi and G. Ananthakrishna, Phys. Rev. E **67**, 065104(R) (2003).

[44] M. S. Bharathi, S. Rajesh, and G. Ananthakrishna, Scr. Mater. **48**, 1355 (2003).

[45] G. Ananthakrishna and M. S. Bharathi, Phys. Rev. E **70**, 026111 (2004).

[46] R. Sarmah and G. Ananthakrishna, Acta Mater. **91**, 192 (2015).

[47] R. De and G. Ananthakrishna, Europhys. Lett. **66**, 715 (2004).

[48] L. D. Landau and E. M. Lifshitz, *Theory of Elasticity* (Pergamon, Oxford, 1986).

[49] R. Sarmah and G. Ananthakrishna, Commun. Nonlinear Sci. Numer. Simulat. **19**, 3880 (2014).

[50] S. Rajesh and G. Ananthakrishna, Phys. Rev. E **61**, 3664 (2000).

[51] G. Ananthakrishna and M. C. Valsakumar, Phys. Lett. A **95**, 69 (1983).

[52] S. J. Noronha, G. Ananthakrishna, L. Quaouire, C. Fressengeas, and L. P. Kubin, Int. J. Bifurcat. Chaos Appl. Sci. Eng. **07**, 2577 (1997).

[53] M. S. Bharathi, M. Lebyodkin, G. Ananthakrishna, C. Fressengeas, and L. P. Kubin, Phys. Rev. Lett. **87**, 165508 (2001).

[54] N. Ranc and D. Wagner, Mater. Sci. Eng. A **394**, 87 (2005).

[55] H. Jiang, Q. Zhang, X. Chen, Z. Chen, Z. Jiang, and X. Wu, Acta Mater. **55**, 2219 (2007).

[56] R. Sarmah, Ph.D. thesis, Indian Institute of Science, Bangalore, India, 2012.

[57] H. G. E. Hentschel and I. Proccacia, Physica D **8**, 435 (1983).

[58] U. Frisch and G. Parisi in *Turbulence and Predictability of Geophysical Flows and Climate Dynamics*, edited by M. Ghil, R. Benzi, and G. Parisi (North-Holland, New York, 1985), p. 84.

[59] K. R. Sreenivasan, Annu. Rev. Fluid. Mech. **23**, 539 (1991).